Assessment of Spatial Variation of the Surface Urban Heat and Cool Island in Sulaymaniyah City during the Dry Season

Hero Nasraldin Mohammed Amin [1], Soran Hmaamin Ahmad [2]
University of Sulaimani,College of Humanities,Department of Geography

DOI: https://doi.org/10.31918/twejer.2473.46
Published: 23/12/2024

Abstract

Urban landscape modifications due to rapid urbanization, thermal capacity and three-dimensional urban geometry as well as climate change can lead to the difference in energy balance and heating capacity between cities and their surroundings and the occurrence of urban heat and cool islands. This study investigated the spatial variation of the surface urban heat island (SUHI) and surface urban cool island (SUCI) in the Sulaymaniyah urban area during the dry season. It examined the spatial variation of Land Surface Temperature (LST) and the SUHI\SUCI intensity through six satellite images of Landsat OLI-TIRS 09 utilized during the period of 21st June to 22nd September 2022. The Mono-Window Algorithm was used to retrieve LST, and the Object-Based Image Analysis (OBIA) was used to classify Land Use\ Land Cover Classes. To find out the key drivers of LST patterns, the related indices such as Normalized Difference Vegetation Index (NDVI), Dry Built-up Index (DBI), Dry Bare Soil Index (DBSI), Normalized Difference Water Index (NDWI), Normalized Soil Moisture Index (NSMI), Evapotranspiration (ET), Albedo and terrain factors (Elevation, Slope, Aspect and Shaded Relief) were computed. The correlation between LST and these indices was examined, and the most negative correlation (r= -0.63) is apparent with NDVI and the positive correlation (r= 0.15) with DBI, the results found that in terms of City-Scale UHI, the overall study area experienced SUCI compared to the non-urbanized 7 km around the city, while Local-Scale method shows that heat and cool islands effect appeared obviously in different LULC of the study area.

Keywords: *LST, SUHI, SUCI, LULC, Biophysical Indices, Terrain Factors*

Assessment of Spatial Variation of the Surface Urban Heat and Cool Island in Sulaymaniyah City during the Dry Season

A.L. Hero Nasraldin Mohammed Amin
University of Sulaimani,College of Humanities,Department of Geography
hero.mohammedamin@univsul.edu.iq
Prof. Dr. Soran Hmaamin Ahmad
University of Sulaimani,College of Humanities,Department of Geography
Soran.amen@univsul.edu.iq

1. Introduction

The variation between the characteristics of land cover and land use in urban and its surrounding areas in terms of geometry, the building materials, absorption of heat, surface albedo and vegetation cover lead to the air and surface temperature differences within an urban core relative to the rural surrounding (Rasul, 2016, p.65). This phenomenon is known as urban heat island (UHI) which refers to the aspect that urban areas are warmer than their rural surroundings (Weng, et. Al., 2004, p.468, EPA, 2008, p.5, Voogt and Oke, 2003, p.372) In contrast, it is an urban cool island (UCI) when the city has lower temperatures compared to its rural surrounding (Miao, et. Al., 2009, p.489). Luke Howard 1833 first recognized the UHI in London (Howard, 1833). The UHI effect is regarded as thermal pollution caused by human activities and as a very influential force in local climate change (Yahaya and Suleiman, 2017, p.239). It can be classified into three, namely; Canopy Urban Heat Island (CUHI); Boundary Urban Heat Island (BUHI); and Surface Urban Heat Island (SUHI). CUHI and BUHI describe the pattern of urban atmospheric warming at a varying altitude above the ground, while SUHI describes the ground-level warming and is caused by the spatial distribution of land surface temperature (LST)(Heisler and Anthony, 2010, p.30 and Stathopoulou, and Constantinos, 2007, p.358) which is the temperature of the skin of Earth's surface(Bechtel, 2015, p.2851 and He, et. Al., 2007, p.2018).

Ground stations are typically used to detect the CUHI by using thermometers to measure air temperature. SUHI is detected depending on remote sensing satellites that capture the spatial patterns of upwelling thermal radiance from which the LST is estimated. The first SUHI observations (from satellite-based sensors) were reported by Rao (1972). Since then, various sensor-platform combinations (satellite, aircraft, ground-based) have been used to make remote observations of the SUHI, or of urban surface temperatures that contribute to SUHI over a range of scales(Voogt and Oke, 2003, p. 273), LST has an obvious impact on analyzing the environmental issues namely urban heat islands, soil moisture and vegetation that play an important role in exchanging bioprocesses of water and energy between the land surface and air, it is also used in studies related to the hydrological cycle, urban climate, climate change, geophysics, evapotranspiration, forest fires, volcano activities and agriculture and environmental monitoring, the heterogeneity of influencing factors such as land cover, vegetation, soil moisture, geology and topography lead to the great spatiotemporal variability of LST(Ibrahim and Haya, 2018, p.175, Faqe Ibrahim, 2017, p.2, Bechtel, 2015, p.2851 and Malik, Jai and Satanand, 2019, p. 25). The measurement of LST driven by LULC classes can provide indications about the extension of thermal distribution related to LULC patterns and human-related changes.

UHI for Sulaymaniyah city is still unexplored, while the city has developed and expanded, especially in the past two decades. Considering the importance of the determination of UHI and related indices, concerning its influence in determining the microclimate in urban areas, it becomes an imperative area of study. Therefore, the present study aims to evaluate the spatial distribution of LST and SUHI\SHCI patterns in Sulaymaniyah City and their spatial relationships with respective indices.

2. Materials and Method

2.1 Study Area

The study area covers the inhabited areas of the six municipalities within the master plan of Sulaymaniyah City in the Eastern part of the Iraqi Kurdistan region and Northeastern Iraq with an area of 197.43 km². It lies between two latitudes 35° 28′ 40″ to 35° 37′ 42″ North and longitudes 45° 12′ 48″ to 45° 30′ 07″ East (Figure 1), it is located in an intermountain plain with elevation ranges between 605 to 1705 m a.s.l., In this study a 7 km distance with an area of 673.93 km² set as buffer zone of the study area.

Figure 1. Location map of the study area

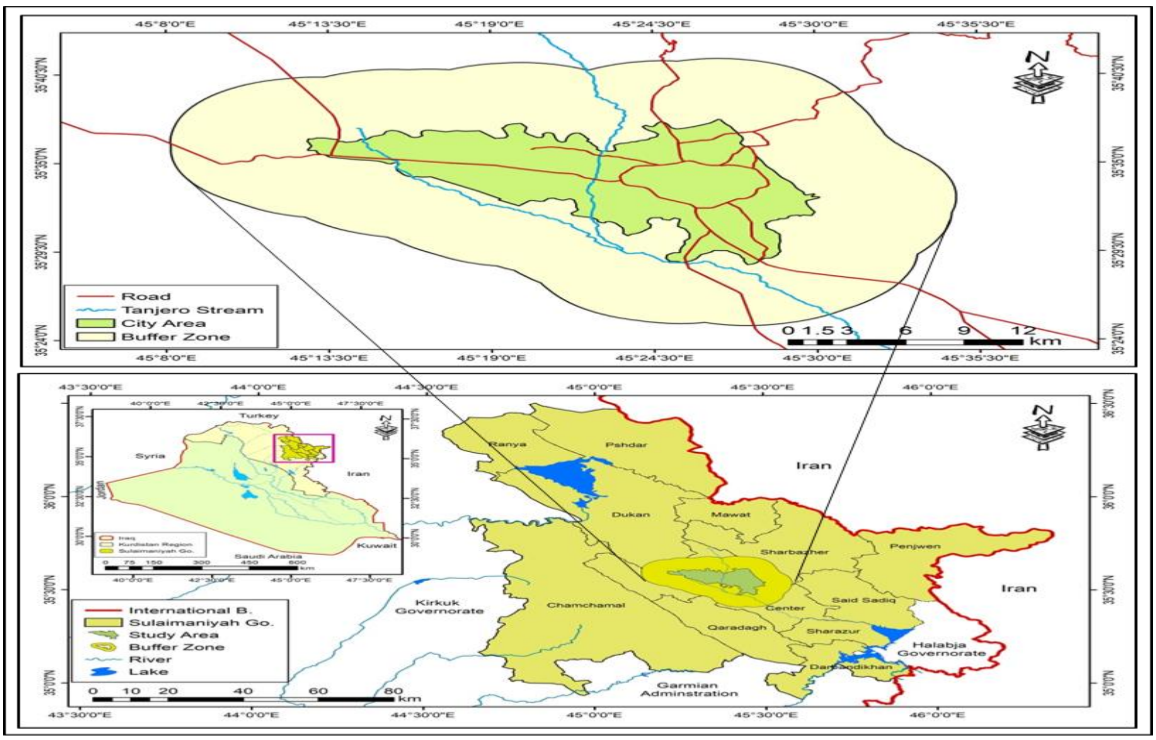

Source: the map prepared using Arc Map 10.8.1 depending on:
- Landsat True colour of the study area.
- Sulaymaniyah Statistical Administration, Master Plan Department, 2022.

2.2 Data

A set of Landsat Operational Land Imager (OLI) / Thermal Infrared Sensor (TIRS) sensors, Path168 \ Row 35 have been used, they were acquired as an image collection of summer 2022 between 21st June to 22nd September 2022 (Table 1). The images were processed and converted to LST and biophysical indices using Google Earth Engine (GEE) cloud-based remote sensing platform, and ArcGIS Spatial Analyst (Version 10.8.1) to get terrain factors through DEM files by Shuttle Radar Topography Mission (SRTM) Global 30 m. It was also used to analyze and export the abovementioned results, and SPSS 22 were used for the statistical analysis computation. To obtain a LULC map, the study primarily relies on the use of a Landsat 8 OLI satellite image with 15m of spatial resolution (after executing the Gram-Schmidt Pan Sharpening processes), that was captured on August 11, 2022, with no cloud cover (0.00). And, the DEM file with 15m spatial resolution of the study area was used as secondary data to produce topographic maps and slope maps, which were used as an auxiliary factor in the classification process (OBIA method), using the ENVI 5.3.0 environment.

Table1. Landsat images used for LST and Biophysical Indices retrieval

Image-Scene-ID	Acquisition Date	Acquisition Time	Sunrise Time	Cloud Cover (%)	Path\Row	Image Quality	Resolution
LC09/C02/T1 (TOA-SR)	25-06-2022	07:32:42 A.M	04:44 (60°)	1.41	168\35	9	30m

LC09/C02/T1 (TOA-SR)	11-07-2022	07:32:38 A.M	04:51 (62°)	0.0	168\35	9	30m
LC09/C02/T1 (TOA-SR)	27-07-2022	07:32:49 A.M	05:02 (65°)	0.0	168\35	9	30m
LC09/C02/T1 (TOA-SR)	12-08-2022	07:33:00 A.M	05:14 (71°)	0.0	168\35	9	30m
LC09/C02/T1 (TOA-SR)	28-08-2022	07:33:03 A.M	05:27 (77°)	0.0	168\35	9	30m
LC09/C02/T1 (TOA-SR)	13-09-2022	07:33:05 A.M	05:39 (85°)	0.01	168\35	9	30m

Source: Images and metadata properties acquired in GEE, and sunrise time detected using Time and Date, Sunrise, Sunset, daylight, Sulaymaniyah, Iraq.

2.3 Methodology

2.3.1. Land surface temperature retrieval

Mono-Window algorithm (MW) (Eq.1) developed by (Qin et al. 2001, 3723) has been used to estimate the LST of Landsat image's thermal infrared band through Google Earth Engine (GEE). Images were resampled to 30m. The algorithm performed atmospheric correction of the Landsat thermal band using atmospheric data provided in GEE, Landsat TIRS bare ground emissivity used to perform surface emissivity correction. The proportion of vegetation (Pv) values for the Landsat image are extracted from NDVI values (Eq.5) and the emissivity of each pixel of the band is extracted using Equation 4.

$$LST = \frac{BT}{\left(1+\left(\lambda * \frac{BT}{p}\right) Ln(\varepsilon)\right)} \qquad (1)$$

LST: Land Surface Temperature
BT: Satellite brightness temperature (°C)
λ: Wavelength of emitted radiance
ε: Surface emissivity for the used channel.
P: is $h \times c/\sigma$ ($1.438\times10-2\ m\ K$), where h is Planck's constant ($6.26\times10-34 J\ s$); c is the speed of light (2.998×108 m/sec); σ is Stefan Boltzmann's constant ($1.38\times10-23 J\ K-1$).

$$BT = \left(\frac{K2}{Ln\left(\frac{K1}{L\lambda}+1\right)}\right) - 273.15 \qquad (2)$$

K1: Calibration Constant 1 from the metadata.
K2: Calibration Constant 2 from the metadata.
$L\lambda$: Top of Atmosphere Spectral Radiance

$$L\lambda = Ml * Qcal + Al \qquad (3)$$

Ml: Band-specific multiplicative rescaling factor from the metadata
Qcal: Digital number of a given pixels
Al: Band-specific multiplicative rescaling factor from the metadata

$$\varepsilon = 0.004 * Pv + 0.986 \qquad (4)$$

0.004: Average emissivity value of bare land
Pv: Proportion of Vegetation
0.986: Values of average emissivity of the vegetated land.

$$Pv = \left(\frac{(NDVI - NDVI\ min)}{(NDVI\ max - NDVI\ min)}\right)^2 \qquad (5)$$

$NDVI_{min}$: NDVI value of fully bare pixels
$NDVI_{max}$: NDVI value of completely vegetated pixels

2.3.2. Quantifying SUHII \ SUCII

The study depends on the standardization of urban heat island intensity to quantify SUHII, it determined the difference of mean LST between the city and the surrounding rural areas as (City-Scale UHI) (Eq.6), following the commonly used procedure (Clinton et al. 2013, Zhou et al., 2014, and Li et al., 2017), (Clinton and Peng, 2013, p. 297, Zhou et. Al., 2014, p. 53, Li, et. Al., 2017, p. 428) also (Local-Scale UHI) (Eq.7) has been used to obtain SUHI \ SUCI of each land use and land cover (LULC) classes using (Unger et al., 2004) (Balazs, Geiger and Sümeghy, 2007, p.8 and Rasul, 2016, p. 76)

$$\Delta LST = LSTu - LSTr \qquad (6)$$

ΔLST: the difference between urban and rural LST
$LSTu$: mean LST of urban area
$LSTr$: mean LST of rural buffer area.
A positive value represents a SUHI situation whilst a negative value represents SUCI intensity.

$$\Delta LST = LSTcell - LSTcell(r) \qquad (7)$$

$LSTcell$: Temperature of the given urban cell
$LSTcell(r)$: Temperature of the rural cell. (This equation has been used to detect UHI based on the mean LST of the city area as well)

Also, the (Coefficient of Variation (C.V)) is used to represent the LST variation ratio within the City area and its buffer zone using the following equation (Abdi, 2010, p.2);

$$C.V = \frac{\text{S.D.}}{\text{Mean}} \times 100$$

$S.D$: Standard Deviation

Urban areas are defined based on the built-up areas within the master plan of the city due to the large expansion of inhabited areas outside the city, a seven-kilometre buffer zone around the city is used to define the reference rural areas' surface temperature. According to LULC obtained from Landsat image for summer 2022, the rural buffer zone consists of a little (2.79%) Built-up pixels, Grassland and Forest cover 43.10% and 26.88% of the whole area, also 18.28%, 7.39% and 0.29% for cropland, barren land and water respectively (Appendix 1).

2.3.3. Computation of biophysical indices and terrain factors

To derive the biophysical parameters of the earth's surface, several spectral indices were calculated on Landsat 09 imagery using the GEE platform. The biophysical indices were represented in this analysis by the normalized difference vegetation index (NDVI), the Dry Built-up Index (DBI), the Dry Bare Soil Index (DBSI), the Normalized Difference Water Index (NDWI), the Normalized Soil Moisture Index (NSMI), Albedo, and Evapotranspiration (ET), (ET formula adopted by Hargreaves and developed by Researcher) (Table 2).

Table 2. Urban and Vegetation Biophysical Indices formula

Biophysical indices	Formula	Source
NDVI	*NDVI= (NIR-Red)/(NIR+Red)*	Sobrino et al., 2004
DBI	*DBI= (Blue – TIRS1/ Blue + TIRS1)-NDVI*	Rasul et al.,2018
DBSI	*DBSI=(SWIR - Green)/(SWIR + Green)-NDVI*	Rasul et al.,2018
NDWI	*NDWI=(NIR-SWIR)/(NIR+SWIR)*	Gao 1995
NSMI	*NSMI=(SWIR1-SWIR2)/(SWIR1+SWIR2)*	Haubrock et al., 2008
ET (mm)	*ET=(0.0023 Ra (T+17.8) √TR)-DBI*	Hargreaves
Albedo	*AL = ((0.356*(Blue)) + (0.130*(Red)) + (0.373*(NIR)) + (0.085*(SWIR1)) + (0.072*(SWIR2))) - (0.0018)) / 1.016*	Liang, S. 2000

The values of NDVI, NDWI, and NSMI vary from -1 and +1, the positive value indicates more vegetated land, more water content, and more moisture content of the soil. As well as the values of DBI and DBSI vary from -2 and +2, the higher numbers represent more built-up and more bare soil area. A DEM file has been used to obtain terrain factors, such as elevation, slope, aspect and a shaded relief map using Arc Map GIS 10.8.1, the data comes from the USGS GloVis (https://glovis.usgs.gov).

2.3.4. Image Classification and Accuracy Assessment

The study primarily relies on the integration of the Machine Learning Method (Support Vector Machine Algorithm-SVM) and Object-Based Image Analysis (OBIA) methodology. The image is radiometric corrected, atmospheric corrected through Flash atmospheric correction and resampled through Gram-Schmidt Pan Sharpening. The SVM algorithm was implemented to distinguish the main classes of the study; about 80 training samples for each class were taken in detail, and 20% of them were identified as truth samples for each class based on information from Google Earth Pro, and SAZ Planet to validate the process. Finally, SVM is executed by using LN kernel functions for LULC mapping. The results obtained by implementing this method have been reused and combined, reclassified with the (OBIA) methodology to obtain the most accurate LULC map, a classification technique is used to assign each object to a land cover class after a series of features (such as spectral, spatial, textural, and contextual ones) are retrieved from each one, and the segmentation procedure was put into place in the first stage for this purpose. However, the scale parameter 70, shape 0.9, and compactness 0.2 of the segmentation procedure were applied to the satellite image. Then the classification procedure is done by gathering and establishing the spectral, spatial, and index information. Each of the indices NDVI, NDWI, and BU (Built-Up Index) has been calculated, and terrain factors have been created from the study area's DEM file. The best value for reclassifying the results and separating the sub-classes has been examined for all of this diverse information in advance.

The study relied on the use of the error matrix technique to evaluate the performance of the classification model, a detailed evaluation process was carried out based on the truth samples for each of the land use/Cover we had determined in the previous stage, the overall accuracy for all applications was 92.8%, and the Kappa coefficient was 0.84, which is considered as an accurate and acceptable result according to previous studies, such as (Feizizadeh, B., 2017 and Feizizadeh, B., et al, 2021)

2.3.5. Statistical Analysis

Due to the spatial variation of LST, the relationship between LST and examined indices was calculated using the Pearson correlation coefficient that provides a standardized measure of linear association between variables, the result ranges from -1 (perfect negative correlation) to +1 (perfect positive correlation) between variables to show the strength of this relationship and displayed as scatterplot with quantifying this relationship with linear regression.

Figure 2. Flowchart Shows the Methodology

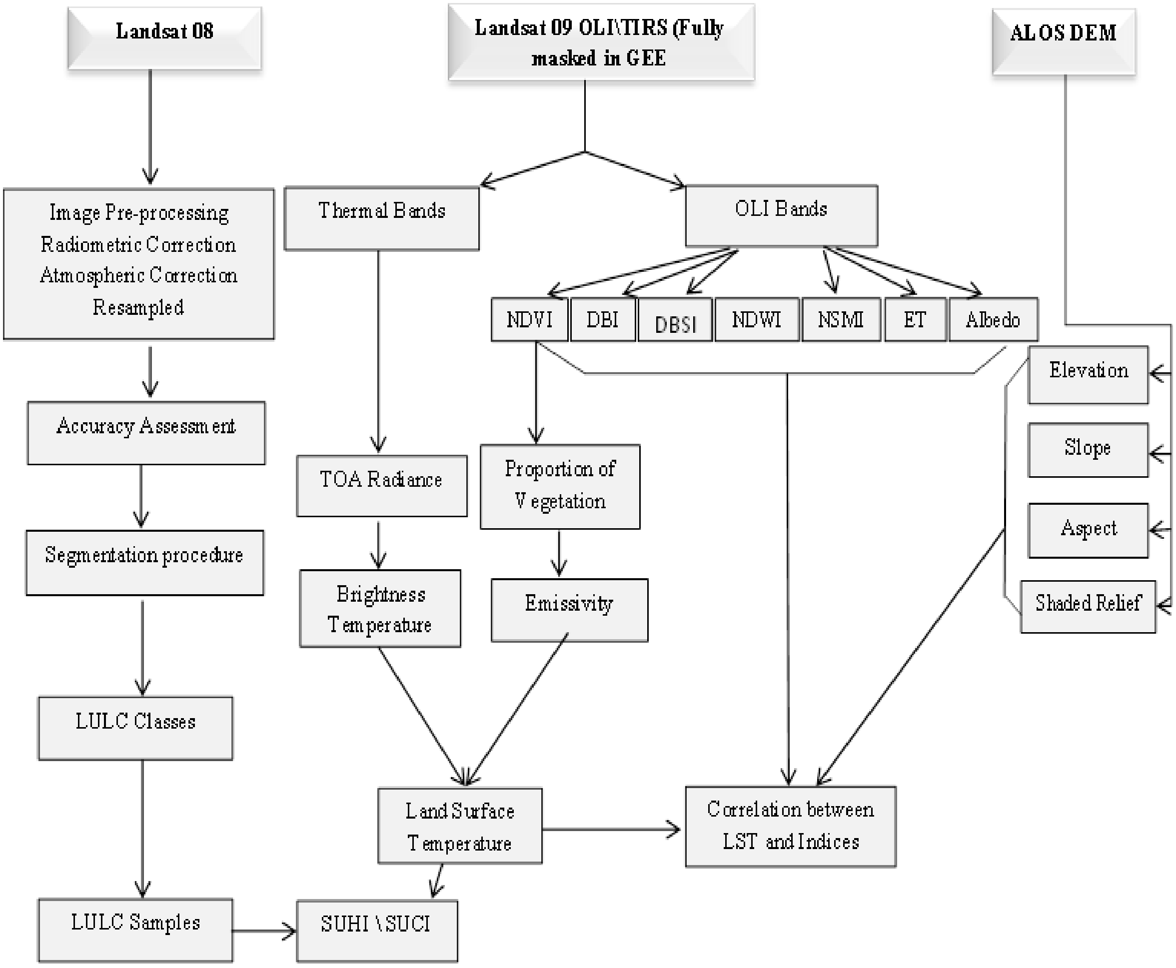

3. Results and Discussion

3.1. SUHII and SUCII in the study area (City-Scale UHI)

The urban-rural temperature contrast is referred to as SUHI\SUCI in the study area. The mean LST of the study area in the morning (at ~ 07:33 A.M) was 40.60 ± 2.54°C, compared to the mean LST of the seven kilometres buffer zone surrounding the city which is 42.33 ± 2.77°C. The UCII of the city is -1.73°C. The percentage of variation between LST values was 6.26% and 6.54% within the city area and buffer zone respectively (Table 3).

Table 3 Summer Land Surface Temperature and UHII\UCII in Sulaymanyiah City

Area	Min LST (°C)	Max LST (°C)	Mean LST (°C)	S.D LST(°C)	C.V	UHII\UCII
City Area	30.22	48.66	40.60	2.54	6.26%	- 1.73
Buffer Zone	28.78	49.75	42.33	2.77	6.54%	

Figure 3. Mean 2022 Summer LST of the study area at 07:33 A.M.

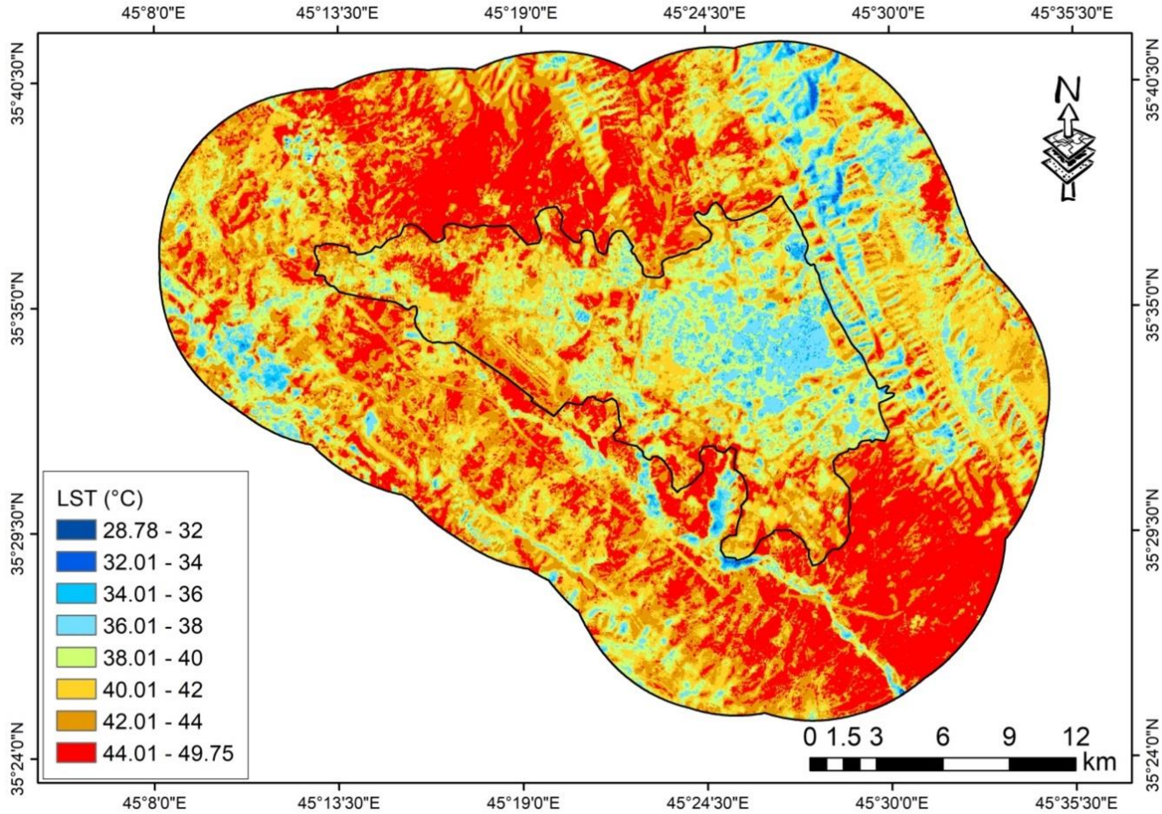

3.2. SUCII and SUHII in selected LULC classes (Local-Scale UHI)

The Local-Scale surface UHI intensity estimation is performed by combining the surface temperature data with the reproduced LULC data (Appendix 2 and Table 4). Mean surface temperatures with standard deviations are calculated for each class by using a zonal statistic tool in GIS operation. In this way, the intensity of SUHI\SUCI is estimated from differences between the mean surface temperature of the different classes and the surrounding rural area of the city and the mean temperature of the city area.

Table 4. The area of Land use \ Land cover classes of the city area

Classes	Area km^2	Ratio %
Built up	106.10	53.74
Industrial Area	10.14	5.14
Road	5.70	2.89
Airport	1.43	0.72
Forest	25.08	12.70
Grassland	13.81	6.99
Cropland	30.72	15.56
Barren Land	4.23	2.14
Water	0.23	0.12
Total	197.43	100.00

Numerous samples as vector data have been selected to present LULC impact on LST and SUHI\SUCI based on definitions of Local Climate Zone proposed by Stewart 2011 (Stewart and Oke, 2012, p. 1885) and the LULC map of the study area using the base map in GIS (Appendix 2 and 3, Table 5).

Table 5. Local-Scale SUHI\SUCI in the study area

LULC Samples	Min LST (°C)	Max LST (°C)	Mean LST (°C)	SD LST(°C)	SUHII\SUCII (Buffer Zone Based)	SUHII\SUCII (Core Based)
Compact Low-Rise LCZ 3	32.45	39.60	36.50	0.78	-5.83	-4.1
Open Low-Rise LCZ 6	35.64	45.60	41.58	1.53	-0.73	+0.98
Compact High-Rise LCZ 1 (E)	32.48	40.97	37	1.54	-5.33	-3.6
Compact High-Rise LCZ 1 (W)	34.87	44.47	39.89	1.73	-2.44	-0.71
Industrial Area	37.43	44.74	41.44	1.03	-0.89	+0.84
Commercial Area	33.61	38.98	37.55	0.78	-4.78	-3.05
Terminal	37.14	41.22	40.21	0.69	-2.12	-0.39
Asphalt Road	34.93	43.20	38.75	1.96	-3.58	-1.85
Airport	36.69	48.66	42.63	1.58	+0.3	+2.03
Park	32.97	39.66	36.89	1.22	-5.44	-3.71
Water Space LCZ G	31.32	36.85	34.85	1.67	-7.48	-5.75
Open Space	39.81	46.82	43.77	1.41	+1.44	+3.17
Grass Land	35.41	38.65	36.76	0.84	-5.57	-3.84
Dense Trees LCZ A	35.87	41.38	37.87	1.13	-4.46	-2.73
Scattered Trees LCZ B	38.61	42.20	40.02	0.63	-2.31	-0.58
Barren Land LCZ F	38.83	47.49	44.66	1.34	+2.33	+4.06
Cropland	39.93	47.03	44.14	1.75	+01.81	+3.54

The SUHI based on buffer zone is associated with the barren land LCZ F +2.33°C, crop land +1.81°C (crops were harvested during the study period which is summer 2022), open space +1.44°C, and Airport +0.3°C classes, the greatest intensity of SUHI was +2.33°C in barren land LCZ F, Lack of vegetation cover, evapotranspiration and soil moisture lead to this warming, while all other classes experienced surface urban cool island, the most intensity values were -7.48°C, -5.83°C, -5.57°C and -5.44°C for water space LCZ G, compact low-rise LCZ 3, grass land and park respectively (Figure 4), at the same time the most intensity heat islands based on mean LST of the city area are in barren land LCZ F +4.06°C, cropland +3.54°C, and +3.17°C and +2.03°C for open space and airport respectively, as well as the most SUCII was -5.75°C for water space LCZ G, - 4.1°C for Compact Low-Rise LCZ 3, and -3.84°C for grass land.

Figure 4. SUHI and SUCI in selected LULC samples for Summer 2022

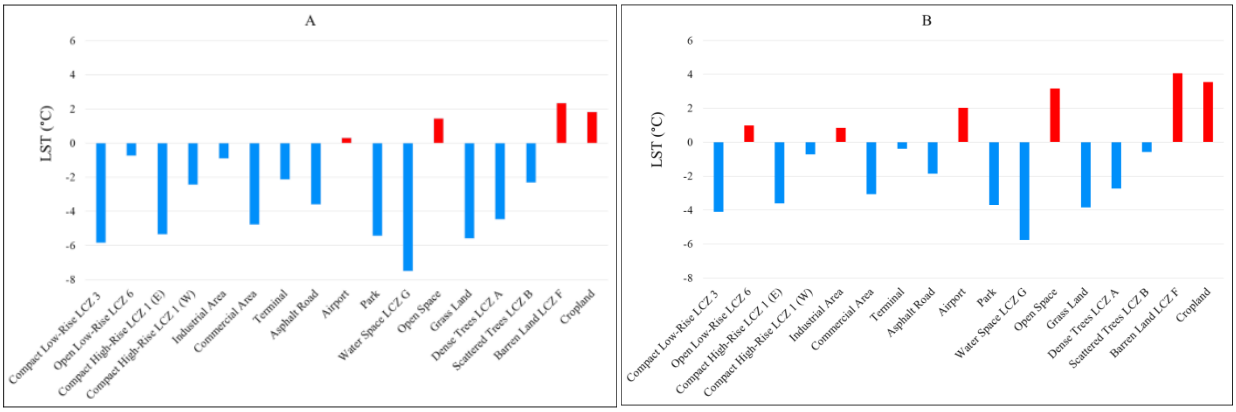

A: is SUHI\SUCI (Buffer Zone based), and B: is SUHI\SUCI (Core based)

3.3. Relationship between LST with Biophysical indices and Terrain factors

In order to determine the relationship between LST and biophysical indices and terrain factors (Appendix 3 and 4); 75 sample points from each index with their LST values were collected, table 6 and 7 show the coefficients of Pearson correlation (r), percentage of the relationship (r^2) and the significant index (P-value).

Table 6. LST- Biophysical indices correlation

Index	.r	r^2	P-value
NDVI	-0.63	0.394	< 0.001
DBI	0.15	0.021	0.235
DBSI	0.13	0.018	0.227
NDWI	-0.13	0.018	0.213
NSMI	-0.56	0.311	< 0.001
ET	-0.51	0.261	< 0.001
Albedo	0.03	0.001	0.735

Table 7. LST- Terrain factors correlation

Terrain factors	.r	r^2	P-value
Elevation	-0.36	0.128	< 0.001
Slope	-0.42	0.175	< 0.001
Aspect	-	0.094	< 0.001
Shaded Relief	-0.58	0.333	< 0.001

Correlation results indicated that LST tends to correlate negatively with most of the indices (Figures 5 and 6; Table 6 and 7), the NDVI had the greatest effect on LST change, which was negatively and significantly correlated with the mean LST r = -0.63, followed by shaded relief r = -0.58, NSMI r = -0.56 and ET r = -0.51, also negative correlation appeared between LST and slope, elevation and NDWI. In contrast, the results obtained from the correlation between LST and DBI, DBSI and Albedo indicated a weak positive correlation, and the correlation between LST and aspect is not obvious, however, LST is higher in eastern aspect compared to other aspects, because the images were taken at 07:33 A.M, and this aspect receives more radiation than the others.

The results show that the correlation between LST and NDVI, NSMI, ET, Elevation, Slope, Aspect and Shaded relief is significant at less than 0.001, while the correlation between LST and other indices is non-significant. Thus, the more the contrast in the biophysical conditions between the urban and the rural, the more intensive the urban heat and cool island would tend to be.

Figure 5. Regression analysis of the LST and biophysical indices

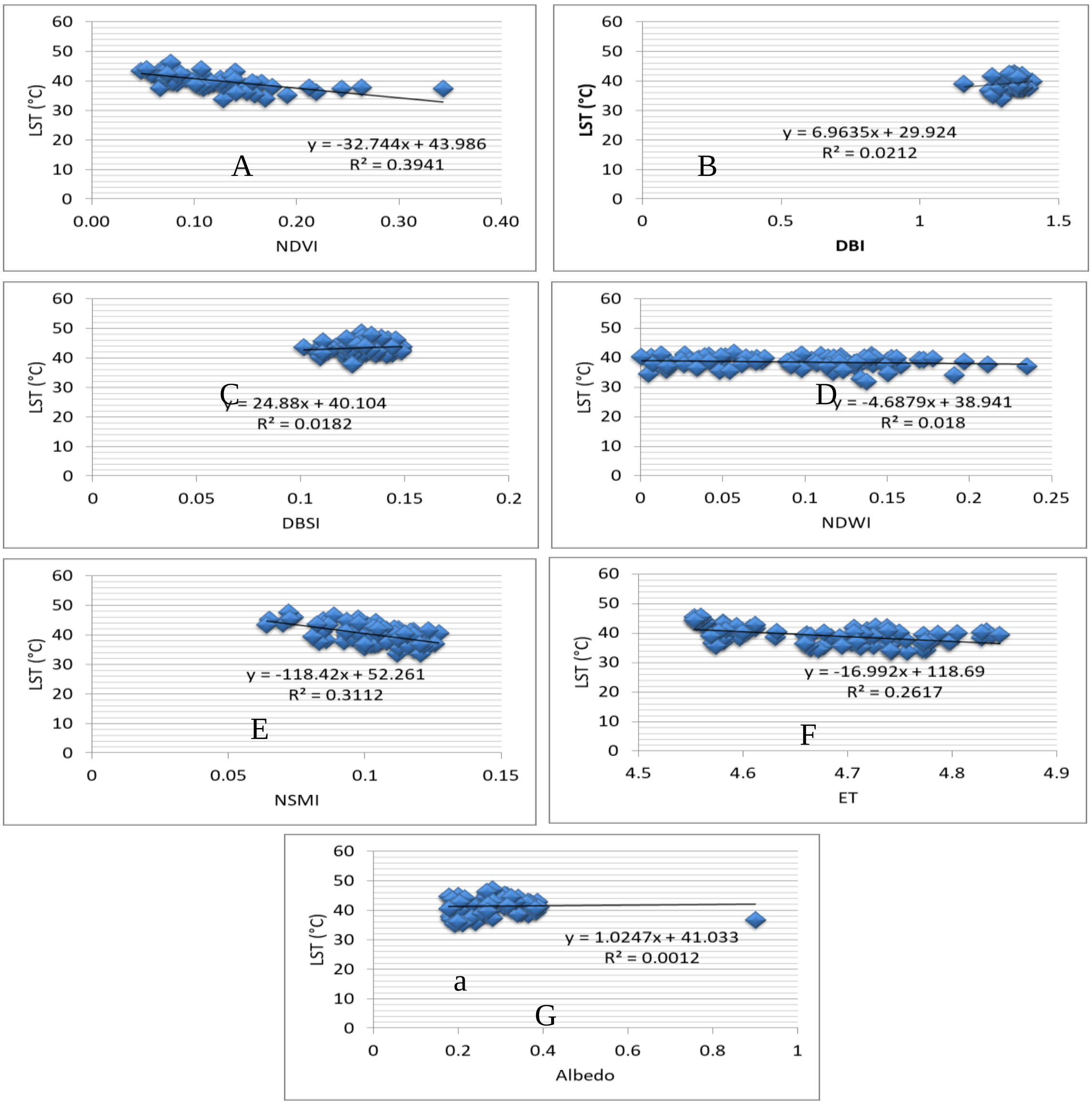

A; represents the regression between (LST-NDVI), B (LST-DBI), C (LST-DBSI), D (LST-NDWI), E (LST-NSMI), F (LST-ET) and G (LST-Albedo).

Figure 6. Regression analysis of the LST and terrain factors

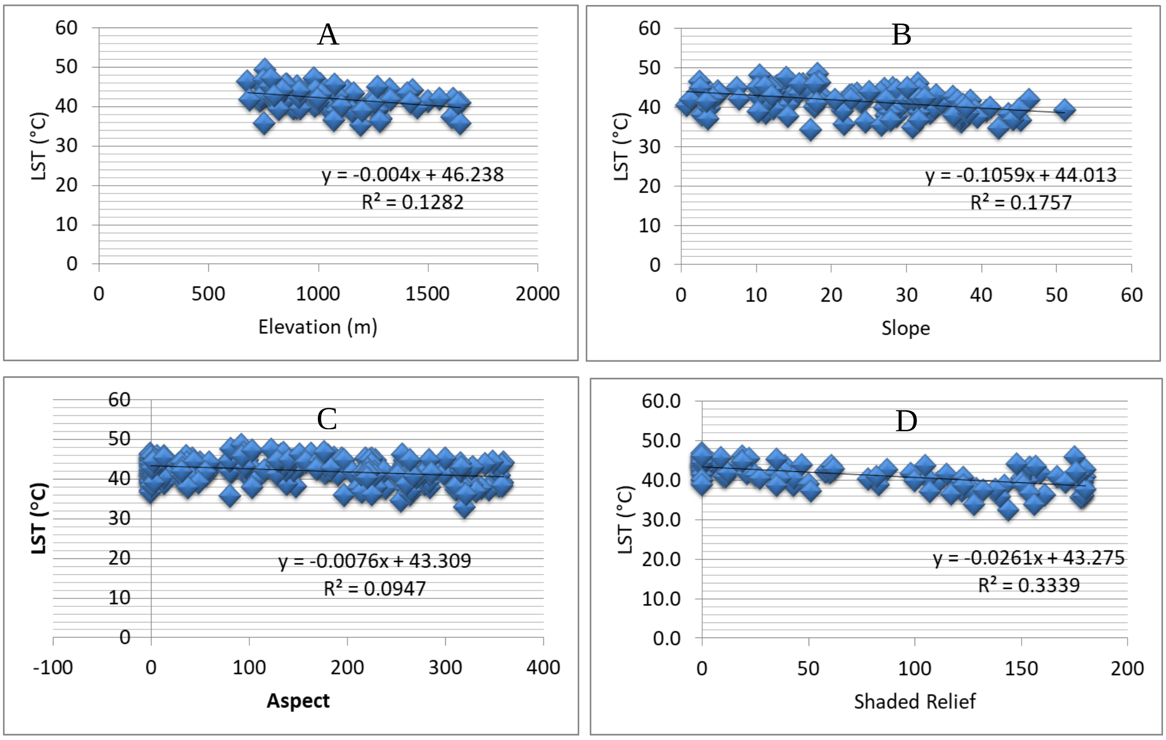

A; represents the regression between (LST-Elevation), B (LST-Slope), C (LST-Aspect) and D (LST-Shaded relief)

Many researchers have studied the relationship between LST and other variables such as vegetation cover, reflective patterns of urban structure (Favretto, 2018, p.219, Grover and Babu, 2015, p. 129 and Voogt and Oke, 2003, p. 376), also land surface temperatures affected by the presence of water bodies and soil moisture (Rasul, 2016, p.125). The temperature and NDVI relationship has long been recognized, and studies have indicated a negative correlation between LST and NDVI, at the same time NDVI alone may not be a sufficient metric to explain UHI quantitatively (Yue, et. Al., 2007, p.3213, Rasul 2016, p.119). The built-up has also been recognized as temperature-raising factors (Weng, 2001, p. 2003, Mohapatra and Changshan, 2010, p.1332). On the other hand, a more reflective surface is known as one of the LST most reducers (Nuruzzaman, 2015, p. 69, Akbari, et. al., 2002, p. 301). Other studies state that terrain factors affect surface temperature, Peng, et. Al., 2020 found that elevation and slope are negatively correlated with LST, the relationship between LST and aspect is not significant, and a significant linear relationship between the values of the shaded relief map and LST. Our results may not agree with these findings completely, because of the time acquisition of the images, which are at (07:33 A.M) and Surface structures differ in the amount of time sufficient for heating and cooling.

4. Conclusion and Recommendation

The summer 2022 LST map for the city of Sulaymaniyah was prepared from Landsat 9 satellite data analysis, which represents the spatial distribution of surface temperature in the city. Overall SUCII of the city was -1.73°C, results have shown higher surface temperature in barren land 44.66 ± 1.34°C and lower in water space 34.85 ± 1.67°C. Generally, the study has recorded the lowest values of LST in the highest values of NDVI, Shaded Relief, NSMI, ET, Slope and Elevation indices and vice versa. While the increase in DBI, DBSI generates a relative increase in LST values, for example, the residential areas with more open space record higher LST than those with lower or no open spaces. Moreover, the variation in temperature between the urban setting and its buffer zone significantly widened. So further studies should investigate more factors and use different satellite images to represent the phenomena carefully.

5. Limitation

The acquisition time of images used in this study is at (07:33 A.M.), and surface structures differ in the amount of time sufficient for heating and cooling, consequently, results show UCI for most of the urban structures, and these results only represent early morning in the study area.

Appendix

Appendix 1. Land Use \ Land Cover Map of the study area and Buffer zone

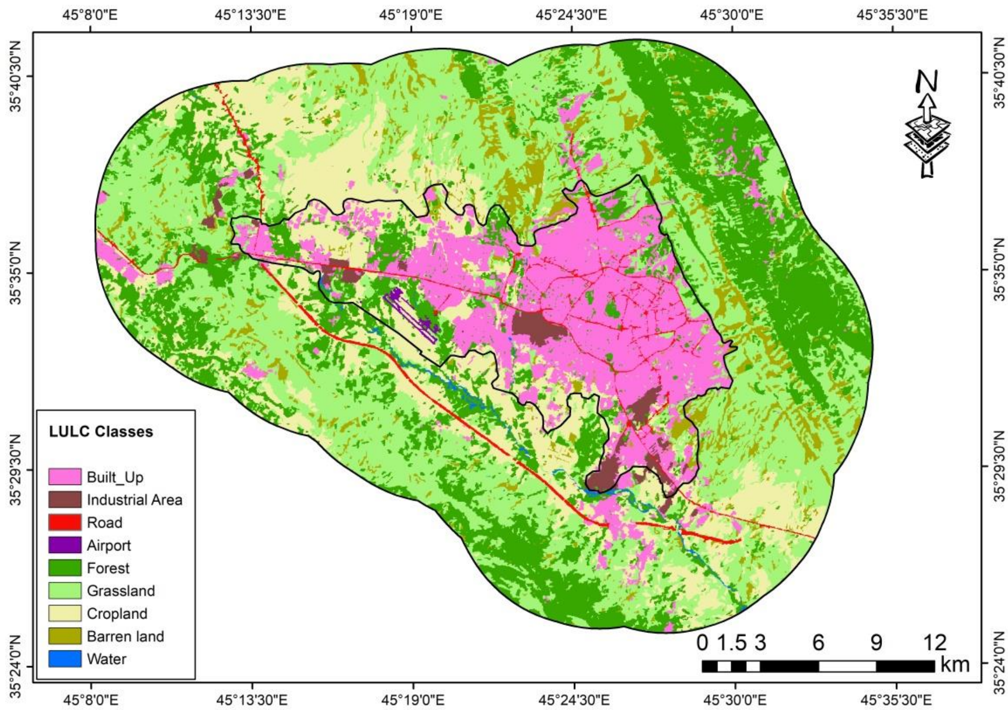

Appendix 2. Selected LULC Samples in the study area

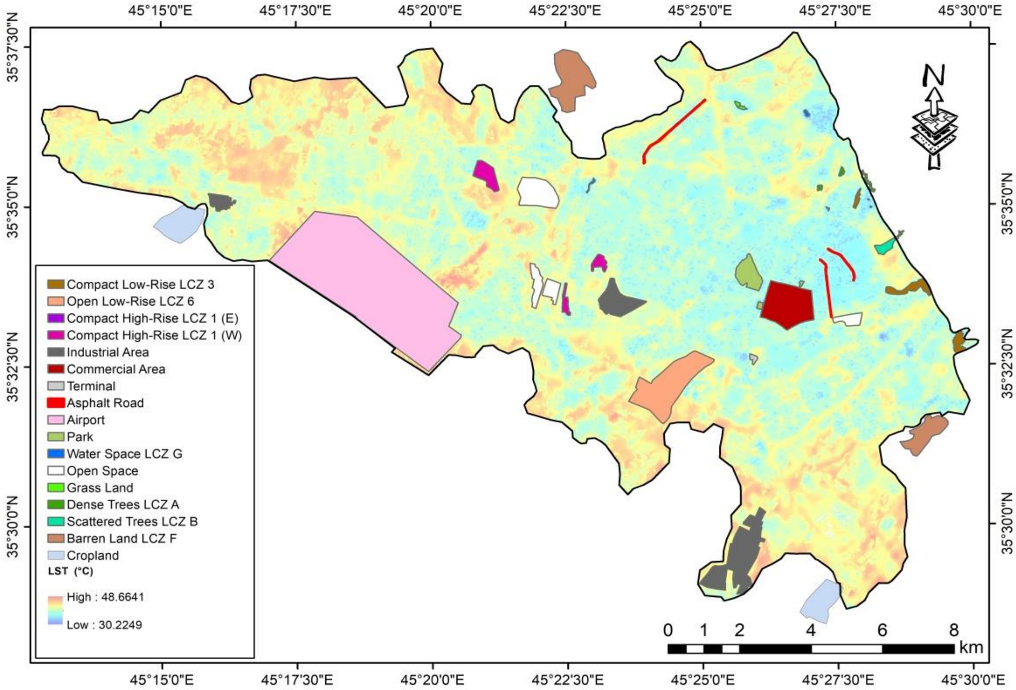

Source: Samples taken depending on base map in Arc GIS 10.8.1

Appendix 3. Samples of Selected LULC in the study area

A: Compact Low-Rise, B: Open Low-Rise, C: Compact High-Rise, D: Industrial Area, E: Commercial Area, F: Terminal, G: Asphalt Road, H: Airport, I: Park, J: Water Space, K: Open Space, L: Grass Land, M: Dense Trees, N: Scattered Trees, O: Barren Land, P: Cropland. (Source: Google Earth Pro, (2021), Maxar Technology).

Appendix 4. Urban Biophysical Indices of the study area

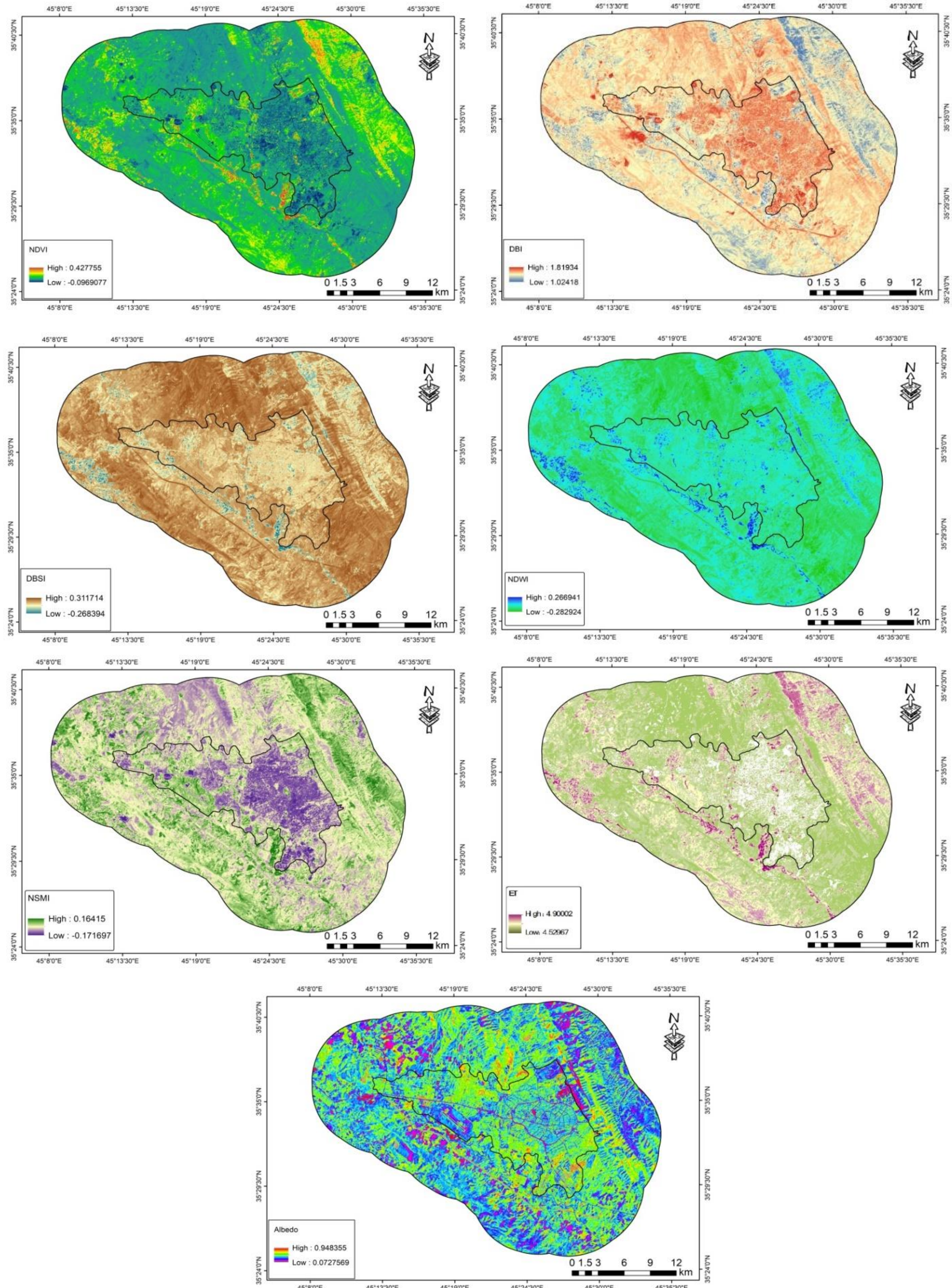

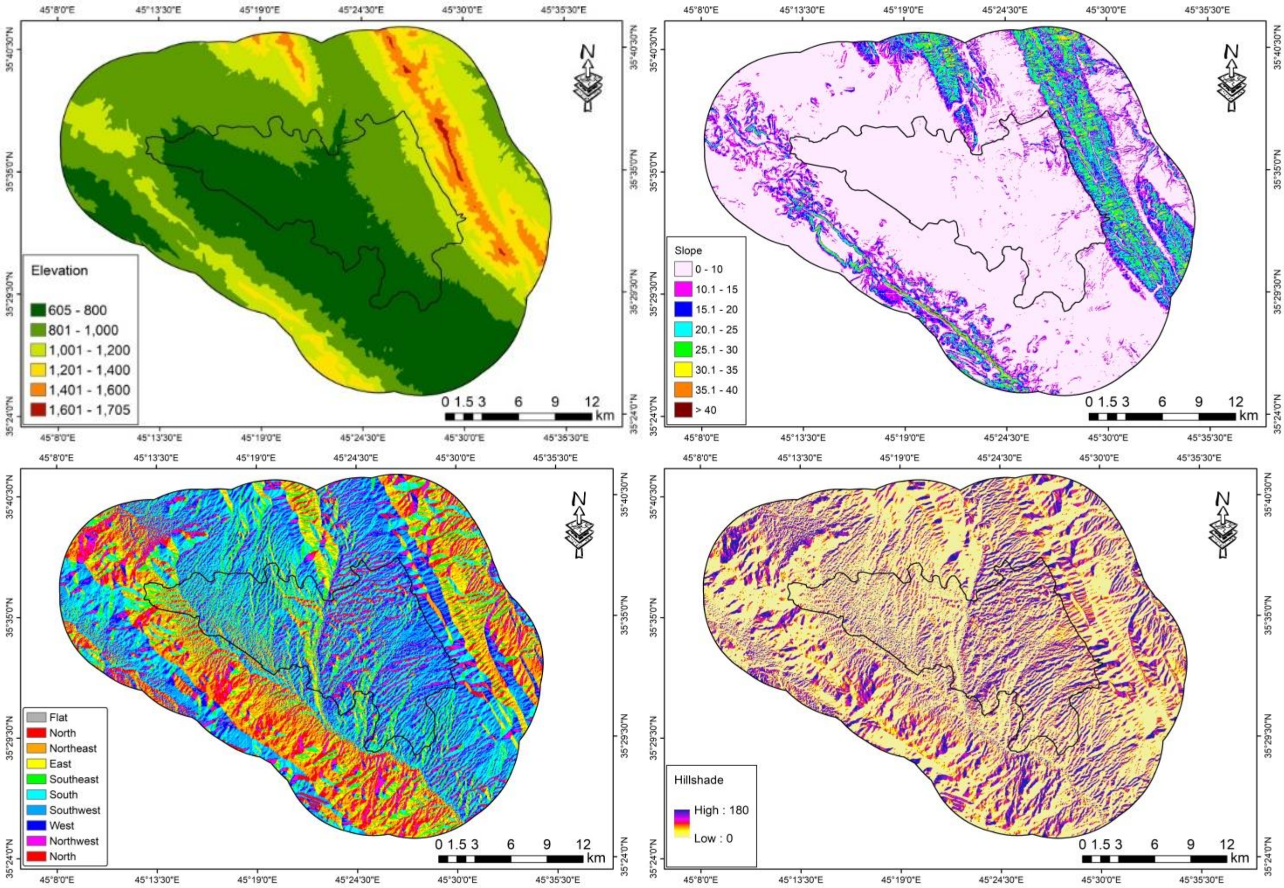

References

Abdi, H., 2010. Coefficient of variation. *Encyclopedia of research design*, *1*(5).

Akbari, H., Pomerantz, M. and Taha, H., 2001. Cool surfaces and shade trees to reduce energy use and improve air quality in urban areas. *Solar energy*, *70*(3), pp.295-310.

Balázs, B., Geiger, J. and Sümeghy, Z., 2007. Annual Mean Urban Heat Island Versus 2D Surface Parameters: Modelling, Validation and Extension. *Acta Climatologica et Chorologica Universitatis Szegediensis, Tomus*, *40*(41), pp.5-15.

Bechtel, B., 2015. A new global climatology of annual land surface temperature. *Remote Sensing*, *7*(3), pp.2850-2870.

Berti, A., Tardivo, G., Chiaudani, A., Rech, F. and Borin, M., 2014. Assessing reference evapotranspiration by the Hargreaves method in north-eastern Italy. *Agricultural Water Management*, *140*, pp.20-25.

Clinton, N. and Gong, P., 2013. MODIS detected surface urban heat islands and sinks: Global locations and controls. *Remote Sensing of Environment*, *134*, pp.294-304.

Epa, U.S., 2008. Reducing Urban Heat Islands: Compendium of Strategies Urban Heat Island Basics. Reducing Urban Heat Islands Compendium of Strategies.

Faqe Ibrahim, G.R., 2017. Urban land use land cover changes and their effect on land surface temperature: Case study using Dohuk City in the Kurdistan Region of Iraq. *Climate*, *5*(1), p.13.

Favretto, A., 2018. Urban Heat Island analysis with Remote Sensing and GIS methods: an application in the Trieste area (North-East of Italy). *Bollettino Della Società Geografica Italiana Serie*, *1*(1), pp.215-229.

Gao, B.C., 1995, June. Normalized difference water index for remote sensing of vegetation liquid water from space. In *Imaging Spectrometry* (Vol. 2480, pp. 225-236). SPIE.

Grover, A. and Singh, R.B., 2015. Analysis of urban heat island (UHI) about normalized difference vegetation index (NDVI): A comparative study of Delhi and Mumbai. *Environments*, *2*(2), pp.125-138.

Haubrock, S.N., Chabrillat, S., Lemmnitz, C. and Kaufmann, H., 2008. Surface soil moisture quantification models from reflectance data under field conditions. *International journal of remote sensing*, *29*(1), pp.3-29.

He, J.F., Liu, J.Y., Zhuang, D.F., Zhang, W. and Liu, M.L., 2007. Assessing the effect of land use/land cover change on the change of urban heat island intensity. *Theoretical and applied climatology*, *90*, pp.217-226.

Heisler, G.M. and Brazel, A.J., 2010. The urban physical environment: Temperature and urban heat islands. *Urban ecosystem ecology*, *55*, pp.29-56.

Howard, L., 1833. *The climate of London: deduced from meteorological observations made in the metropolis and at various places around it* (Vol. 3). Harvey and Darton, J. and A. Arch, Longman, Hatchard, S. Highley [and] R. Hunter.

Ibrahim, M. and Abu-Mallouh, H., 2018. Estimate land surface temperature about land use types and geological formations using spectral remote sensing data in Northeast Jordan. *Open Journal of Geology*, *8*(2), pp.174-185.

Sobrino, J.A., Jimenez-Munoz JC dan Paolini L. 2004. *Land surface temperature retrieval from Landsat TM*, *5*, pp.434-40.

Li, X., Zhou, Y., Asrar, G.R., Imhoff, M. and Li, X., 2017. The surface urban heat island response to urban expansion: A panel analysis for the conterminous United States. *Science of the Total Environment*, *605*, pp.426-435.

Liang, S., 2001. Narrowband to broadband conversions of land surface albedo I: Algorithms. *Remote sensing of environment*, *76*(2), pp.213-238.

Malik, M.S., Shukla, J.P. and Mishra, S., 2019. Relationship of LST, NDBI and NDVI using Landsat-8 data in Kandaihimmat watershed, Hoshangabad, India.

Miao, S., Chen, F., LeMone, M.A., Tewari, M., Li, Q. and Wang, Y., 2009. An observational and modelling study of characteristics of urban heat island and boundary layer structures in Beijing. *Journal of Applied Meteorology and Climatology*, *48*(3), pp.484-501.

Mohapatra, R.P. and Wu, C., 2010. High-resolution impervious surface estimation: An integration of IKONOS and Landsat-7 ETM+ imagery. *Photogrammetric Engineering and Remote Sensing*, *76*(12), pp.1329-1341.

Mohapatra, Rama Prasada, and Changshan Wu. "High-resolution impervious surface estimation: An integration of IKONOS and Landsat-7 ETM+ imagery." Photogrammetric Engineering and Remote Sensing 76, no. 12 (2010): 1329-1341.

Peng, X., Wu, W., Zheng, Y., Sun, J., Hu, T. and Wang, P., 2020. Correlation analysis of land surface temperature and topographic elements in Hangzhou, China. *Scientific Reports*, *10*(1), p.10451.

Qin, Z., Karnieli, A. and Berliner, P., 2001. A mono-window algorithm for retrieving land surface temperature from Landsat TM data and its application to the Israel-Egypt border region. *International journal of remote sensing*, *22*(18), pp.3719-3746.

Rasul, A., 2016. *Remote sensing of surface urban cool and heat island dynamics in Erbil, Iraq, between 1992 and 2013* (Doctoral dissertation, University of Leicester).

Rasul, A., Balzter, H., Ibrahim, G.R.F., Hameed, H.M., Wheeler, J., Adamu, B., Ibrahim, S.A. and Najmaddin, P.M., 2018. Applying built-up and bare-soil indices from Landsat 8 to cities in dry climates. *Land*, *7*(3), p.81.

Sobrino, J.A., Jiménez-Muñoz, J.C. and Paolini, L., 2004. Land surface temperature retrieval from LANDSAT TM 5. *Remote Sensing of Environment*, *90*(4), pp.434-440.

Stathopoulou, M. and Cartalis, C., 2007. Daytime urban heat islands from Landsat ETM+ and Corine land cover data: An application to major cities in Greece. *Solar Energy*, *81*(3), pp.358-368.

Stewart, I.D. and Oke, T.R., 2012. Local climate zones for urban temperature studies. *Bulletin of the American Meteorological Society*, *93*(12), pp.1879-1900.

Voogt, J.A. and Oke, T.R., 2003. Thermal remote sensing of urban climates. *Remote sensing of environment*, *86*(3), pp.370-384.

Weng, Q., Lu, D. and Schubring, J., 2004. Estimation of land surface temperature–vegetation abundance relationship for urban heat island studies. *Remote sensing of Environment*, *89*(4), pp.467-483.

Weng, Q., 2001. Remote sensing? GIS evaluation of urban expansion and its impact on surface temperature in the Zhujiang Delta, China. *International journal of remote sensing*, *22*(10), pp.1999-2014.

Yahaya, T.I. and Suleiman, Y.M., 2017. Urbanisation Effect on the Occurrence of Urban Heat Island over Kano Metropolis, Nigeria.

Yue, W., Xu, J., Tan, W. and Xu, L., 2007. The relationship between land surface temperature and NDVI with remote sensing: application to Shanghai

Landsat 7 ETM+ data. *International journal of remote sensing*, *28*(15), pp.3205-3226.

Zhou, D., Zhao, S., Liu, S., Zhang, L. and Zhu, C., 2014. Surface urban heat island in China's 32 major cities: Spatial patterns and drivers. *Remote sensing of environment*, *152*, pp.51-61.

پوختە

گۆڕانکاری لە دیمەنی شارەکاندا بەهۆی خێرایی زیادبوونی شارنشینی و توانای گەرمی و ئەندازەی سێ ڕەهەندی شارەکان و هەروەها گۆڕانی ئاووهەوا دەتوانێت ببێتەهۆی جیاوازی هاوسەنگی وزە و توانای گەرمکردن لەنێوان شارەکان و دەوروبەریان و ڕوودانی دوورگەی گەرمی و ساردی شار. ئەم توێژینەوەیە لێکۆڵینەوەی لە جیاوازی شوێنیی دوورگەی گەرمی ڕووری زەوی (SUHI) و دوورگەی ساردی ڕووی زەوی (SUCI) لە شاری سلێمانی لە وەرزی وشکدا کردووە. تێیدا جیاوازی شوێنی پلەی گەرمی ڕووی زەوی (LST) و توندی دوورگەی سارد و گەرمی SUCI\SUHI لەڕێگەی شەش وێنەی مانگی دەستکردی لاندسات (OLI-TIRS,09) کە لەماوەی نێوان ٢١ی حوزەیران تا ٢٢ی ئەیلولی ٢٠٢٢ گیراون، خراوەتەڕوو بە بەکارهێنانی ئەلگۆریتمی تاك-پەنجەرە (Mono-Window Algorithm)، پاشان پۆلێنکردنی بەکارهێنانی زەوی و ڕووپۆشی زەوی لەڕێگەی میتۆدی(OBIA) . بەمەبەستی دۆزینەوەی بزوێنەرە سەرەکییەکانی پلەی گەرمی ڕووی زەوی، پێوانە پەیوەندیدارەکانی وەکو پێوانەی ڕووەك (NDVI) ، پێوانەی زەوی بنتیاتنراو(DBI) و پێوانەی خاکی ڕووتەنی وشك(DBSI) ، پێوانەی ئاو(NDWI) ، شێی خاك(NSMI) ، بەهەڵمبوون وئاودەردان (ET) ، ئەلبیدۆ و فاکتەرەکانی بەرزونزمی وەکو (بەرزی، لێژی، ئاراستەی لێژی و سێبەری بەرزونزمی) بۆ ناوچەکە دۆزراوەتەوە. پەیوەندی نێوان LST و ئەم پێوانانە دۆزرانەوە ، دەرکەوت زۆرترین پەیوەندی پێچەوانە (r= -0.63) لەگەڵ NDVI و زۆرترین پەیوەندی ڕاستەوانە (r= 0.15) لەگەڵ DBI بووە، ئەنجامەکان ئەوەیان دەرخست کە بەشێوەیەکی گشتی و بە بەراورد بە ٧کم لە دەوروبەری شارەکەدا کە شارنشین نەبووە دوورگەی سارد لە شارەکەدا دەرکەوتووە، لە کاتێکدا بەپێی شێوازی لۆکاڵی لە دیاریکردنی دوورگەی گەرمی دەرکەوت کە کاریگەری دوورگەی گەرم و سارد بە ئاشکرا لە بەکارهێنان و ڕووپۆشە جیاوازەکانی زەوی ناوچەی لێکۆڵینەوەدا دەرکەوتوون.

کلیلە وشەکان: LST، SUHI، SUCI، LULC پێوانە بایۆفیزیکییەکان، فاکتەرەکانی بەرزوونزمی

الملخص

التغييرات في المشهد الحضري بسبب التحضر السريع والقدرة الحرارية والهندسة الحضرية ثلاثية الأبعاد بالإضافة إلى تغير المناخ تؤدي إلى اختلاف توازن الطاقة وقدرة التدفئة بين المدن والمناطق المحيطة بها وحدوث جزيرة الحرارية والجزيرة الباردة. تبحث هذه الدراسة عن التباين المكاني لجزيرة الحرارية الحضرية السطحية (SUHI) و جزيرة الباردة الحضرية السطحية (SUCI) في مدينة السليمانية خلال موسم الجاف. تم استخدام ست صور من Landsat OLI-TIRS 09 خلال الفترة من ٢١ حزيران إلى ٢٢ ايلول لاستخراج التباين المكاني لدرجة حرارة سطح الأرض (LST) ، وشدة الجزيرة الحرارية و الباردة SUHI \ SUCI ، استخدم خوارزمية النافذة الأحادية (Mono-Window Algorithm) لاسترداد درجة الحرارة السطح ، و تم التصنيف فئات استخدام الأرضي / الغطاء الأرضي باستخدام (OBIA). و لمعرفة الدوافع الرئيسية لأنماط درجة الحرارة السطحية، تم تحليل المؤشرات ذات الصلة مثل مؤشر النباتي (NDVI) ، مؤشر البناء الجاف (DBI) ، مؤشر التربة الجافة العارية (DBSI) ، مؤشر المياه (NDWI) ، رطوبة التربة الطبيعية (NSMI)، التبخر والنتح (ET) ، وعوامل البيدو والتضاريس (الارتفاع ، الانحدار ، اتجاه انحدار ، والتضاريس المظللة). تم تحليل الارتباط بين LST وهذه المؤشرات ، وكان الارتباط الأكثر سلبية ($r = -0.63$) مع NDVI و الارتباط الإيجابي ($r = 0.15$) مع DBI ، و وجدت النتائج ظهور الجزيرة الباردة في المدينة من حيث الفرق بين متوسط درجة الحرارة المدينة و ٧ كم غير الحضرية حول المدينة، بينما أظهرت طريقة المقياس المحلي أن تأثير الجزر الحرارية والجزر الباردة ظهر بشكل واضح في استخدامات والغطاءات الارضية المختلفة في منطقة الدراسة.

الكلمات المفتاحية: LST، SUHI، SUCI، LULC ، المؤشرات البيوفيزيكية ، عوامل التضاريس